

**Electronic structure of titania aerogels from soft x-ray absorption spectroscopy**

S. O. Kucheyev,\* T. van Buuren, T. F. Baumann, J. H. Satcher, Jr., T. M. Willey, R. W. Meulenberg, T. E. Felter, J. F. Poco, S. A. Gammon, and L. J. Terminello  
*Lawrence Livermore National Laboratory, Livermore, California 94550, USA*

(Received 17 February 2004; published 3 June 2004)

The electronic structure of TiO<sub>2</sub> aerogels is studied by soft x-ray absorption near-edge structure (XANES) spectroscopy. High-resolution O *K*-edge and Ti *L*<sub>2,3</sub>-edge XANES spectra of aerogels are compared with those of rutile, anatase, and unrelaxed amorphous phases of full-density TiO<sub>2</sub>. Results show that all the main spectroscopic features of aerogels, reflecting the element-specific partial density of empty electronic states and correlation effects, can be attributed to the absence of long-range order in stoichiometric amorphous TiO<sub>2</sub>. Based on these results, we discuss the effects of short- and long-range order on the electronic structure of TiO<sub>2</sub>.

DOI: 10.1103/PhysRevB.69.245102

PACS number(s): 71.20.Be, 78.70.Dm, 71.23.Cq, 82.70.Rr

**I. INTRODUCTION**

Titanium dioxide (TiO<sub>2</sub>) is currently the most studied single-crystal transition metal oxide in the field of surface science.<sup>1</sup> Significant research interest in TiO<sub>2</sub> has been fueled by its numerous technological applications, including heterogeneous catalysis, solar cells, optical and corrosion coatings, gas sensors, varistors, and pigments in paints and cosmetic products.<sup>1</sup> Several polymorphic forms of TiO<sub>2</sub> crystals can exist at ambient conditions, with tetragonal rutile and anatase being the most common phases. A stoichiometric amorphous phase of TiO<sub>2</sub> can also be stabilized at ambient conditions. Recently, various forms of nanostructured TiO<sub>2</sub>, such as nanoparticles, xerogels, and aerogels, have been synthesized and have attracted significant research interest.<sup>1,2</sup> Our interest in this work is focused on a somewhat extreme form of *nanoporous titania*—TiO<sub>2</sub> aerogels, which are open-cell solid foams derived from highly cross-linked gels by drying them under supercritical conditions.<sup>2</sup> Titania aerogels are typically characterized by a high degree of porosity, with ultrafine (nanometer size) cells/pores.<sup>2-4</sup>

Since many applications of TiO<sub>2</sub> are based on the specific surface and/or bulk electronic properties, numerous previous studies have been focused on understanding electronic structure of different forms of titania.<sup>1</sup> In particular, x-ray absorption near-edge structure (XANES) spectroscopy and electron energy loss spectroscopy (EELS) have been used to probe element-specific partial density of empty electronic states in different polymorphs of full-density TiO<sub>2</sub>.<sup>1</sup> However, as will be discussed in detail below, physical mechanisms responsible for the difference in XANES spectra of different polymorphs of TiO<sub>2</sub> are still not well understood.

Recently, Ti *K*-edge XANES has also been applied to study TiO<sub>2</sub> xerogels.<sup>5-7</sup> Such Ti *K*-edge studies of TiO<sub>2</sub> are typically focused on the analysis of relatively broad, low-intensity pre-edge peaks, which are assumed to be related to the crystal field symmetry around Ti atoms. There are still debates regarding assignment of these pre-edge features in Ti *K*-edge XANES spectra to particular core-level electron transitions.<sup>5-7</sup> In contrast, the Ti *L*<sub>2,3</sub>-edge features (in the soft x-ray regime) are typically much better resolved and significantly more sensitive to the local bonding configurations (reflecting the valency of Ti and the geometry of its

surroundings) than the Ti *K*-edge features.<sup>1</sup> However, we are not aware of previous Ti *L*<sub>2,3</sub>-edge XANES studies of titania xerogels or any previous XANES studies of titania aerogels. Hence, in this paper, we present a high-resolution XANES study of titania aerogels and compare results with those for rutile, anatase, and amorphous phases of full-density TiO<sub>2</sub>. We show that all the main spectroscopic features of aerogels can be attributed to the absence of long-range order in stoichiometric amorphous TiO<sub>2</sub> (*a*-TiO<sub>2</sub>). We also show that some features of Ti *L*<sub>2,3</sub>-edge XANES spectra which have previously been assigned to effects of oxide reduction<sup>1,8-10</sup> can be attributed to the absence of long-range order in stoichiometric *a*-TiO<sub>2</sub> and are indicative of the presence of an amorphous phase.

**II. EXPERIMENTAL**

The following samples were investigated in this study: two titania aerogels with average densities of 180 and 370 mg/cm<sup>3</sup> (i.e., ~4 and 9% of the full density), rutile and anatase powders (with grain sizes  $\geq 5\mu\text{m}$ ) purchased from Sigma-Aldrich Corp., and (001)-oriented rutile single crystals obtained from Princeton Scientific Corp.

**A. Aerogel synthesis and structural characterization**

The TiO<sub>2</sub> aerogels were prepared by a two-step sol-gel process that involved acid-catalyzed hydrolysis of titanium ethoxide [Ti(OEt)<sub>4</sub>], followed by base-initiated gelation of the titania species. In a typical synthesis, titanium ethoxide (7.0 g, 31 mmol) was dissolved in absolute ethanol (25 mL), and the solution was chilled in an ice bath with vigorous stirring. When cool, the reaction solution was treated with hydrochloric acid (37%, 0.5 mL) and then distilled water (0.6 mL). After five minutes, propylene oxide (2.5 g, 43 mmol) was added to the solution. The reaction mixture was stirred for an additional five minutes, then transferred to glass molds, and, within 2 h, translucent white alcogels formed. The titania alcogels were allowed to age at room temperature for 72 h before being dried in a Polaron<sup>TM</sup> critical point extractor. The ethanol in the pores of the wet gels was exchanged with liquid CO<sub>2</sub> for 3–4 days, after which time, the temperature was ramped up to ~45 °C, while

maintaining a pressure of  $\sim 100$  bar. The autoclave was then depressurized at a rate of  $\sim 7$  bar/h, affording the titania aerogels as opaque white monoliths.

The bulk densities of the aerogels were determined by measuring the dimensions and mass of monolithic samples. The microstructure of aerogels was studied by x-ray diffraction (XRD) and high-resolution transmission electron microscopy (TEM). The TEM analysis was performed in a Philips CM300FEG transmission electron microscope operating at 300 kV using zero loss energy filtering with a Gatan energy imaging filter to remove inelastic scattering. The TEM images were taken under bright-field (BF) conditions and slightly defocused to increase contrast.

### B. Preparation of amorphous $\text{TiO}_2$

A sample of full-density  $\alpha$ - $\text{TiO}_2$  was prepared by bombardment of a (001)-oriented rutile single crystal at 77 K with 340 keV  $^{132}\text{Xe}^{2+}$  ions to a dose of  $1.5 \times 10^{15} \text{ cm}^{-2}$  with a beam flux of  $\sim 2 \times 10^{12} \text{ cm}^{-2} \text{ s}^{-1}$ . During bombardment, the sample was tilted by  $\sim 7^\circ$  relative to the incident ion beam to minimize channeling. Previous studies<sup>11–13</sup> have shown that bombardment under such conditions results in the formation of a continuous surface amorphous layer. Our Rutherford backscattering-channeling spectrometry analysis at LLNL (with 2 MeV  $^4\text{He}$  ions) suggested that the thickness of the surface amorphous layer in the implanted rutile sample was  $\sim 200$  Å. The as-implanted sample was not subjected to any high-temperature processing, and stoichiometrical changes due to ion-beam-induced (preferential) sputtering were negligible for such a relatively low ion dose ( $1.5 \times 10^{15} \text{ cm}^{-2}$ ).<sup>14,15</sup> Hence, the  $\sim 200$ -Å-thick surface layer in this sample is composed of unrelaxed stoichiometric  $\alpha$ - $\text{TiO}_2$ .<sup>16,17</sup>

### C. X-ray absorption

The XANES experiments were performed at undulator beamline 8.0 at the Advanced Light Source (ALS), Lawrence Berkeley National Laboratory. Details of the beamline have been published elsewhere.<sup>18</sup> Aerogels and  $\text{TiO}_2$  powders were pressed into an indium metal foil and mounted on the sample holder. All spectra presented in this paper were obtained by measuring the total electron yield (TEY), by monitoring the total sample photocurrent, as a function of photon energy scanned through O  $K$  and Ti  $L_{2,3}$  edges. It should be noted that measurements in the total fluorescence yield (TFY) mode revealed the same spectral features for all the samples studied (but with the expected worse signal-to-noise ratio). All absorption measurements were performed at room temperature. The incoming radiation flux was monitored by the total photocurrent produced in a clean Au mesh inserted into the beam. The overall experimental resolution around the Ti  $L_{2,3}$  edge was  $\sim 150$  meV. The monochromator was calibrated by aligning the Ti  $L_3$  and O  $K$  edges of a rutile single crystal according to the EELS values reported by Brydson *et al.*<sup>19</sup> After a background subtraction, all spectra were normalized to the post-edge step heights. To extract peak positions, each spectrum was fitted with a set of Lorentzian functions with a linear background.<sup>20</sup>

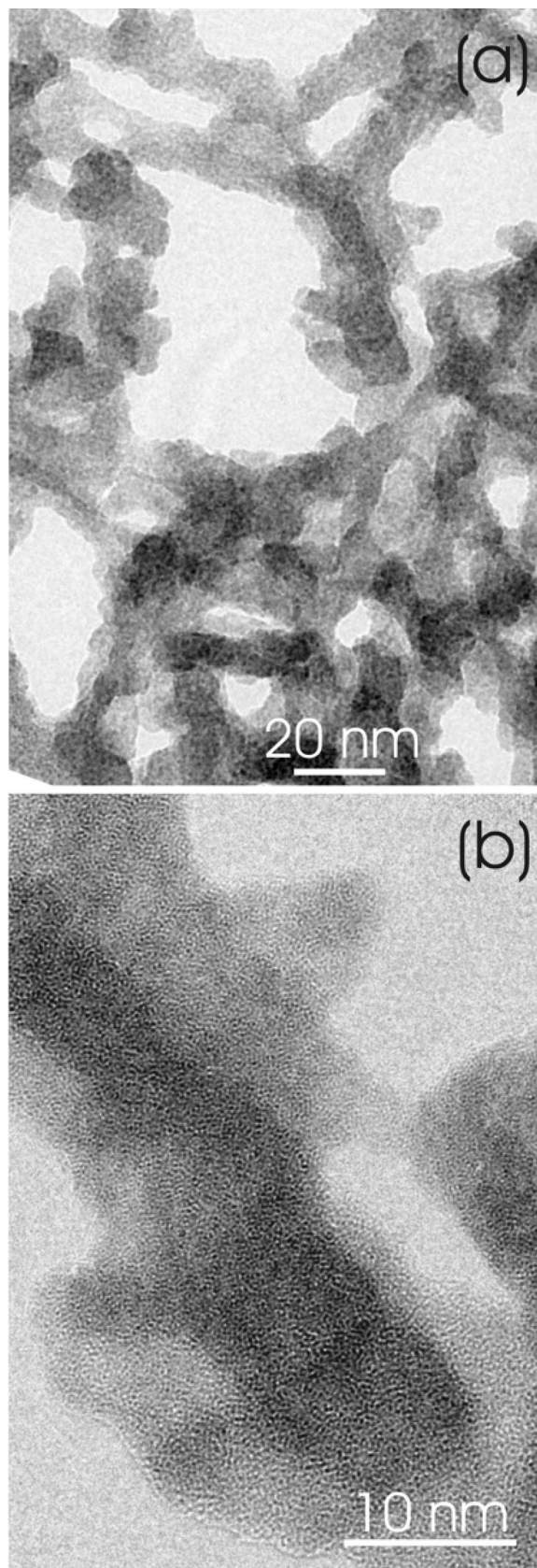


FIG. 1. High-resolution TEM images of a titania aerogel (with a density of  $180 \text{ mg/cm}^3$ ) at different magnifications.

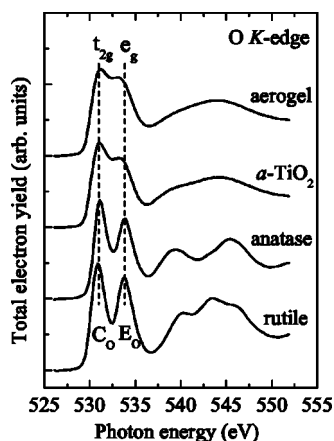


FIG. 2. Oxygen *K*-edge XANES spectra of rutile, anatase, amorphous  $\text{TiO}_2$  (*a*- $\text{TiO}_2$ ), and a titania aerogel.

### III. RESULTS AND DISCUSSION

#### A. Microstructure of aerogels

Before the XANES study, the morphology of the two titania aerogels was studied by XRD and TEM. Our XRD analysis showed that both aerogels were fully amorphous, with no evidence for the presence of either rutile or anatase phase. The morphology of aerogels was further characterized by TEM. Figure 1(a) shows a BF TEM image illustrating how irregular  $\text{TiO}_2$  particles of  $\sim 10$ – $20$  nm in size are interconnected to form a treelike structure of the aerogel. In agreement with XRD results, our selected-area diffraction analysis has confirmed that the aerogels are fully amorphous. The amorphous structure of the aerogel can also be seen in a high-resolution image in Fig. 1(b). It should be noted that the morphology of amorphous aerogels studied in this paper (see Fig. 1) is rather different from that reported previously in Refs. 3 and 4. Indeed,  $\text{TiO}_2$  aerogels synthesized by Zhu *et al.*<sup>3</sup> consisted of  $\sim 5$  nm anatase particles closely packed into mesoaggregates  $\sim 30$  nm in size, whereas those reported by Masson *et al.*<sup>4</sup> were composed of faceted anatase particles  $\sim 30$  nm in size. Such a difference in the structure and morphology (and, hence, the properties) of titania aerogels reported in different studies can be attributed to differences in conditions of aerogel synthesis.

#### B. Soft x-ray absorption

It should be noted that peak positions in both Ti and O edge XANES spectra were almost identical for the two aerogels studied. Likewise, no significant difference was found between peak positions in rutile spectra for powders and

single crystals. Hence, for brevity, in this paper, we show spectra for only one aerogel (with a density of  $370 \text{ mg/cm}^3$ ) and single-crystal rutile.

#### 1. Oxygen *K* edge

Figure 2 gives a comparison of O *K*-edge XANES spectra of rutile, anatase, *a*- $\text{TiO}_2$ , and an aerogel. Spectra of rutile and anatase, shown in Fig. 2, are in general agreement with results of a number of previous XANES and EELS studies.<sup>1,8–10,19,21–24</sup> It is seen from Fig. 2 that, for all the  $\text{TiO}_2$  polymorphs studied, spectra exhibit two main peaks centered on  $\sim 531$  and  $534$  eV (labeled  $C_O$  and  $E_O$ , whose positions are given in Table I) with an additional structure at higher energies. A slight shift of peak  $C_O$  to larger energies (by  $\sim 0.2$  eV) in anatase as compared to the case of rutile can be seen from Fig. 2 and Table I, which could be attributed to a larger bandgap<sup>1</sup> of anatase ( $3.2$  eV) as compared to that of rutile ( $3.0$  eV).

Figure 2 and Table I also show that spectra of *a*- $\text{TiO}_2$  and an aerogel are very similar, suggesting that the (electronic) structure of the titania aerogels studied in this work is similar to that of stoichiometric *a*- $\text{TiO}_2$ . All the peaks in spectra of an aerogel and *a*- $\text{TiO}_2$  are broadened as compared to the case of rutile (single-crystal and powder) and anatase (powder). Such an inhomogeneous broadening, due to slight variations in bond lengths and angles, is inherent to spectra from amorphous solids. A significant decrease in the distance between  $C_O$  and  $E_O$  peaks from  $\sim 3.0$  to  $2.3$  eV upon amorphization can also be seen from Fig. 2 and Table I. Note that such a decrease is caused by the shift of peak  $E_O$  to lower energies, while, for both *a*- $\text{TiO}_2$  and an aerogel, peak  $C_O$  is at the same energy as for rutile.

Previous electronic band structure calculations have shown that O *K*-edge XANES and EELS spectra of rutile and anatase can be well explained with single-electron approximation models.<sup>22</sup> These spectra essentially map the O  $2p$ -projected density of empty states in  $\text{TiO}_2$ .<sup>22</sup> Correlation effects appear to have a negligible influence on the O *K*-edge spectra since O  $2p$  states are hybridized and relatively delocalized, resulting in their weak interaction with the O  $1s$  core hole (i.e., a reduced screening of the electric field from the nucleus due to the absence of the electron at the core level).

In the molecular orbital (MO) picture of  $\text{TiO}_2$ ,<sup>19,21,22,25</sup> the bonding between Ti  $4sp$  and O  $2p$  orbitals forms the (mostly O  $2p$  derived) valence band. The conduction band, which is probed in XANES experiments, is formed by anti-bonding Ti  $3d$ ,  $4s$ , and  $4p$  and O  $2p$  orbitals. In addition, the crystal field of the surrounding O atoms splits the Ti  $3d$  band into  $t_{2g}$  (formed by  $d_{xy}$ ,  $d_{xz}$ , and  $d_{yz}$  orbitals) and  $e_g$

TABLE I. Peak positions (in eV) in O *K*-edge and Ti  $L_{2,3}$ -edge XANES spectra, as labeled in Figs. 2–4.

	$C_O$	$E_O$	A	B	$C_3$	$D_3$	$E_3$	$C_2$	$D_2$	$E_2$	$F_3$	$G_3$	$F_2$	$G_2$
Rutile	530.9	533.9	456.6	457.3	458.2	460.0	461.1	463.8	465.7	466.5	471.4	473.3	477.0	479.2
Anatase	531.1	533.9	456.7	457.4	458.3	460.1	461.0	463.8	465.9	466.7	471.6	473.6	477.1	479.2
<i>a</i> - $\text{TiO}_2$	530.9	533.2	456.6	457.4	458.2	459.8	460.6	463.7	465.6	466.3	471.0	472.7	476.8	478.6
Aerogel	530.9	533.1	456.6	457.4	458.2	459.8	460.6	463.7	465.6	466.6	471.1	472.9	476.7	478.5

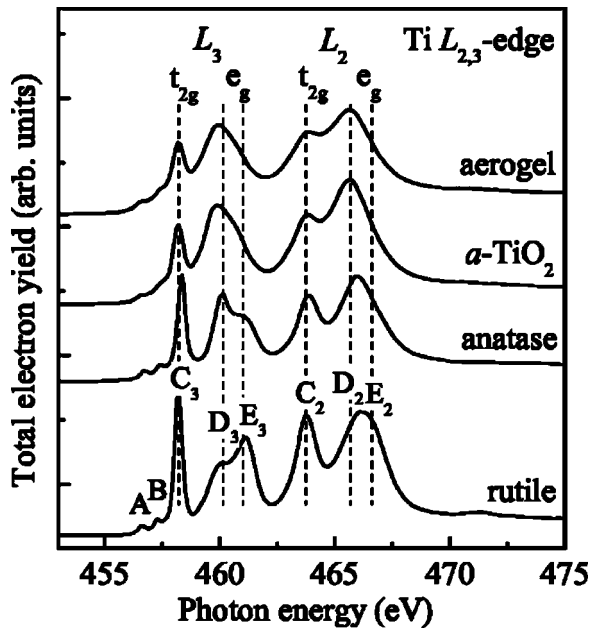


FIG. 3. Titanium  $L_{2,3}$ -edge XANES spectra of rutile, anatase, amorphous  $\text{TiO}_2$  ( $a\text{-TiO}_2$ ), and a titania aerogel. See Table I for the positions of the peaks labeled.

(formed by  $d_{x^2-y^2}$  and  $d_{z^2}$  orbitals) subbands. Since the Ti  $e_g$  orbitals point directly toward the  $2p$  orbitals of the surrounding O atoms, the  $e_g$  band is very sensitive to the local environment. The  $e_g$ -related peaks are also expected to be broader than the  $t_{2g}$  peaks due to a larger degree of hybridization of the Ti  $e_g$  orbitals with O ligands and associated effects of solid-state broadening, which has been discussed in detail in Ref. 22.

Within the MO picture, the two main peaks  $C_0$  and  $E_0$  in Fig. 2 can be attributed to the excitation from the O  $1s$  core level into the  $t_{2g}$  and  $e_g$  bands, respectively, and peaks at higher energies are due to transitions into antibonding O  $2p$  and Ti  $4sp$ -related bands.<sup>19,21,22,25</sup> The ligand-field splitting can be estimated from the energy difference between the  $t_{2g}$  and  $e_g$  features in O  $K$ -edge spectra,<sup>22</sup> giving  $\sim 3.0$  and  $2.8$  eV for rutile and anatase, respectively. Table I also shows that the ligand-field splitting is further reduced to  $\sim 2.3$  eV in  $a\text{-TiO}_2$  and an aerogel, which is caused by a shift in the position of the  $e_g$  related peak  $E_0$ . This is consistent with the fact that the  $e_g$  orbitals are more sensitive to the local environment than the  $t_{2g}$  orbitals, and we will come back to this effect in the next section.

## 2. Titanium $L_{2,3}$ edge

Figure 3 compares high-resolution Ti  $L_{2,3}$ -edge XANES spectra of a titania aerogel and different  $\text{TiO}_2$  polymorphs. In contrast to the O  $K$ -edge spectra discussed above, Ti  $L_{2,3}$ -edge spectra, reflecting transitions of Ti  $2p$  core electrons into Ti  $3d$  states in the conduction band, show a considerably more complex behavior. Such complexity arises from correlation effects (which are described beyond the independent electron approximation). Indeed, atomic multiplet calculations of de Groot *et al.*<sup>26,27</sup> have suggested that the

multiplet structure, discussed below, is mainly due to strong Coulomb interactions between poorly screened Ti  $3d$  electrons and the Ti  $2p$  core hole.

In Fig. 3, peaks for all  $\text{TiO}_2$  polymorphs are split into two groups, separated by  $\sim 5.5$  eV, due to the spin-orbit coupling of Ti  $2p$  core electrons, giving rise to  $L_2$  and  $L_3$  edges. The  $L_2$ -edge features are broadened compared to those of the  $L_3$  edge, owing to the increased Coster-Kronig Auger decay channel for the  $L_2$  edge (i.e., a shorter lifetime of the  $2p_{1/2}$  core hole due to a radiationless electron transition from the  $2p_{3/2}$  to the  $2p_{1/2}$  level, accompanied by the promotion of a valence electron into the conduction band). For both  $L_2$  and  $L_3$  edges, the crystal field splits the  $3d$  band into  $t_{2g}$  and  $e_g$  subbands, as discussed in Sec. III B 1. As in the case of O  $K$ -edge spectra in Fig. 2, the  $t_{2g}$ -related peaks  $C_2$  and  $C_3$  for anatase in Fig. 3 are slightly shifted to higher energies as compared to cases of rutile,  $a\text{-TiO}_2$ , and an aerogel. Such a shift (which has often been overlooked in previous XANES and EELS studies due to insufficient experimental resolution) could be attributed to the difference in bandgaps of rutile and anatase. It should also be noted that, according to calculations of de Groot *et al.*,<sup>22,26</sup> the distance between  $t_{2g}$  and  $e_g$  related peaks in Ti  $L_{2,3}$ -edge spectra does not represent the crystal field splitting since these spectra are strongly affected by correlation effects.

Figure 3 also shows that, for all  $\text{TiO}_2$  polymorphs, the  $e_g$ -related peak of the  $L_3$  edge is further split into two peaks, labeled  $D_3$  and  $E_3$ . A similar splitting of the  $e_g$  band (into  $D_2$  and  $E_2$  peaks) also occurs for the  $L_2$  edge, although it is not well resolved due to the lifetime-related broadening of the  $L_2$  edge. Indeed, Fig. 3 clearly shows that an increase in the  $D_3/E_3$  intensity ratio in transition from rutile to anatase to  $a\text{-TiO}_2$ /aerogel is followed by a shift of the broad  $L_2$  edge  $e_g$  peak to lower energies. This is consistent with the scenario when the  $e_g$  band of the  $L_2$  edge is composed of two peaks ( $D_2$  and  $E_2$ ), whose intensities follow the intensities of better resolved  $D_3$  and  $E_3$  peaks. This is also supported by results of our peak deconvolution/fitting (see Table I).

According to atomic multiplet calculations of de Groot *et al.*<sup>26</sup> for rutile and anatase, low-intensity peaks A and B in Fig. 3, mixed into the  $L_3$  edge and weakly affected by ligand field, are a result of the strong interaction between poorly screened  $3d$  electrons and the  $2p$  core hole. However, recent band structure calculations by Finkelstein *et al.*<sup>28</sup> suggest that these pre-edge peaks A and B can also be attributed to sharp features in the (one-electron) Ti  $3d$  partial density of states, while the widths and intensities of these peaks are modified by correlation effects. Hence, additional theoretical studies are presently needed to better understand the origin of these pre-edge peaks A and B.

Figure 3 and Table I show that, as in the case of the O  $K$ -edge spectra discussed above, Ti  $L_{2,3}$ -edge spectra of an aerogel and  $a\text{-TiO}_2$  are very similar. It is also seen from Fig. 3 that, upon amorphization, in addition to the expected broadening of all peaks, the intensity of peaks  $E_2$  and  $E_3$  is largely reduced, and the  $e_g$  band for both  $L_2$  and  $L_3$  edges is dominated by  $D_2$  and  $D_3$  peaks, which are also slightly shifted to lower energies. This results in significant overall

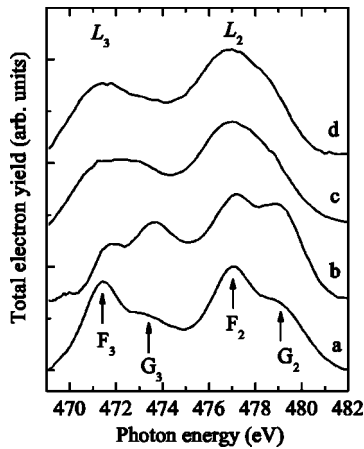


FIG. 4. High-energy region of Ti  $L_{2,3}$ -edge XANES spectra of rutile (a), anatase (b), amorphous  $\text{TiO}_2$  (c), and an aerogel (d). The curves were obtained by a background subtraction from  $L_{2,3}$ -edge XANES spectra such as shown in Fig. 3.

shifts of the broad  $L_2$ -edge  $e_g$ -related peak to lower energies for  $a$ - $\text{TiO}_2$  and an aerogel. Figure 3 and Table I also show that the positions of  $t_{2g}$ -related peaks A, B, and C in an aerogel and  $a$ - $\text{TiO}_2$  are close to those in rutile rather than in anatase.

Figure 4 shows the higher-energy region of Ti  $L_{2,3}$ -edge XANES spectra of different  $\text{TiO}_2$  polymorphs after the subtraction of the contribution from Lorentzian  $D_2$  and  $E_2$  peaks.<sup>29</sup> Peaks in Fig. 4 are split into two groups (labeled  $F_3$ ,  $G_3$  and  $F_2$ ,  $G_2$  and given in Table I), separated by  $\sim 5.5$  eV, suggesting that these are due to transitions from the  $2p_{3/2}$  ( $L_3$  edge) and  $2p_{1/2}$  ( $L_2$  edge) core levels. It is seen from Fig. 4 that, in the amorphous phase (spectra c and d), all four peaks appear to be present but are broadened, which makes a more detailed peak analysis rather challenging. Within the MO approach,<sup>19,25</sup> this higher-energy structure, which is  $\sim 13.3$  eV above the first major peaks of the Ti  $L_{2,3}$  edge (peaks  $C_2$  and  $C_3$  in Fig. 3), can be attributed to a transition from the Ti  $2p$  core levels to  $t_{1u}$ -type orbitals of rutile and anatase. One-electron calculations of Finkelstein *et al.*<sup>28</sup> for rutile have suggested (although not totally convincingly) that these peaks could be attributed to some features of the Ti  $3d$  density of states. An alternative (and even more speculative) explanation, proposed over a decade ago by van der Laan,<sup>24</sup> is that these higher-energy peaks for rutile and anatase are a result of a polaronic-type transition of an electron from the valence band to the conduction band, accompanying the core-level x-ray absorption process. It is clear that, at present, additional theoretical work is needed to better understand the origin of these higher-energy  $L_{2,3}$ -edge peaks in  $\text{TiO}_2$  polymorphs.

Figure 3 and Table I have shown that the major difference between Ti  $L_{2,3}$ -edge spectra of amorphous and crystalline phases of  $\text{TiO}_2$  is a significant change in positions, intensities, and widths of  $e_g$ -related peaks D and E. Therefore, we discuss the splitting of the  $e_g$ -related band in more detail below. Different physical mechanisms have previously been proposed to explain the splitting of the  $e_g$  band (into D and E peaks) in Ti  $L_{2,3}$ -edge spectra of rutile and anatase. In atomic

multiplet calculations of de Groot *et al.*,<sup>26</sup> this splitting has been produced by a distortion of the symmetry around Ti atoms from the perfect  $O_h$  (octahedral) to  $D_{2h}$  and  $D_{2d}$  by an amount to fit experimental XANES spectra for rutile and anatase, respectively. However, this concept has seriously been questioned by Crocombette and Jollet,<sup>30</sup> who, by taking into account the exact positions of O atoms in the first-neighbor shell of Ti, have demonstrated that the amount of lattice distortion used by de Groot *et al.*<sup>26</sup> is unrealistic.

In an alternative explanation proposed by Brydson *et al.*,<sup>19</sup> the splitting of the  $e_g$  band may be attributed to the dynamic Jahn-Teller effect (due to the coupling of the electronic and vibrational states). However, the actual values of the splitting observed in optical absorption experiments of  $\text{Ti}^{3+}$  ions in the octahedral environment in different systems and attributed to the Jahn-Teller effect are much smaller than the relatively large separation ( $\sim 1$  eV) of peaks D and E in Fig. 3. For example, the splitting of the  $e_g$  doublet measured by optical absorption in the  $\text{Al}_2\text{O}_3:\text{Ti}^{3+}$  system is  $\sim 0.3$  eV at 300 K.<sup>31</sup> Moreover, the splitting due to the Jahn-Teller effect has a characteristic temperature dependence: it decreases with decreasing temperature. By analogy with the  $\text{Al}_2\text{O}_3:\text{Ti}^{3+}$  system,<sup>31</sup> the splitting of the  $e_g$ -related peak in XANES spectra would be expected to decrease by  $\sim 50\%$  with decreasing sample temperature from 300 to 77 K if it were due to the Jahn-Teller effect. In contrast, our XANES study of rutile (single-crystal) and anatase (powders) reveals a negligible change in positions of D and E peaks upon decreasing sample temperature to 77 K. This strongly suggests that the Jahn-Teller effect is not a major contributor to the splitting of the  $e_g$ -related band in Ti  $L_{2,3}$ -edge XANES spectra of  $\text{TiO}_2$  polymorphs.

Another explanation for the  $e_g$  band splitting has recently been given by Finkelstein *et al.*<sup>28</sup> based on their band structure calculations, suggesting that the splitting of the  $e_g$  band in rutile could simply be related to the particular shape of the Ti  $3d$  partial density of states. This could also be inferred from the partial density of states related to the  $e_g$  subband of rutile calculated earlier by Munnix and Schmeits<sup>32</sup> using a tight-binding method. However, only rutile has been studied in Refs. 28 and 32, and rather different densities of states for rutile (and anatase) have been predicted by other calculations (see, for example, Refs. 22,33–35). Hence, attributing difference in the  $e_g$  band splitting in different polymorphs of  $\text{TiO}_2$  to variations in the (one-electron) partial density of states should currently await further theoretical studies.

Finally, the splitting of the  $e_g$  band can also be attributed to effects of long-range order, and in particular, to the influence of the interactions of Ti with the second-neighbor shell.<sup>19,30</sup> This mechanism seems to be supported by results of the present study, showing that significant changes occur to XANES spectra as a result of amorphization (i.e., loss of long-range order). It is also interesting to note that, although the Ti  $L_{2,3}$ -edge spectra of  $a$ - $\text{TiO}_2$ /aerogel are significantly different from those of both rutile and anatase, the  $e_g$ -related peaks in spectra of  $a$ - $\text{TiO}_2$ /aerogel are more similar to those of anatase rather than rutile. This could be attributed to the fact that, according to previous extended x-ray absorption fine structure (EXAFS) studies,<sup>5–7,36,37</sup> the local atomic ar-

rament in amorphous titania is similar to that in anatase rather than in rutile (particularly for the second coordination shell). Although this supports the importance of longer-range order in the interpretation of XANES spectra of TiO<sub>2</sub> polymorphs, additional (quantitative) theoretical studies are desirable to better understand the effect of long-range order on the electronic structure of titania.

#### IV. CONCLUSIONS

In conclusion, we have studied the electronic structure of amorphous TiO<sub>2</sub> aerogels by high-resolution soft x-ray absorption spectroscopy around O *K* and Ti *L*<sub>2,3</sub> edges. The main conclusions of this work can be summarized as follows.

(i) All the main spectroscopic features of amorphous aerogels are the same as those of full-density amorphous TiO<sub>2</sub>. Hence, these spectroscopic features are indicative of the absence of long-range order in TiO<sub>2</sub>. It is not necessary to

invoke oxide reduction, as has previously been done to interpret similar features in XANES spectra of full-density titania.<sup>1,8–10</sup>

(ii) The local order in amorphous TiO<sub>2</sub>, which can be conveniently probed by soft x-ray absorption, is more similar to that in anatase rather than in rutile.

(iii) The splitting of the *e<sub>g</sub>*-related band in Ti *L*<sub>2,3</sub>-edge XANES spectra of TiO<sub>2</sub> polymorphs is attributed to effects of long-range order. However, additional (quantitative) theoretical studies are currently needed to support this assignment as well as to explain the appearance of high-energy peaks in Ti *L*<sub>2,3</sub>-edge XANES spectra of TiO<sub>2</sub> polymorphs.

#### ACKNOWLEDGMENT

This work was performed under the auspices of the U.S. Department of Energy by the University of California, Lawrence Livermore National Laboratory under Contract No. W-7405-Eng-48.

\*Email address: kucheyev1@llnl.gov

<sup>1</sup>See, for example, recent reviews by U. Diebold, *Surf. Sci. Rep.* **48**, 53 (2003); J.G. Chen, *ibid.* **30**, 1 (1997).

<sup>2</sup>See, for example, T. F. Baumann, A.E. Gash, G.A. Fox, J.H. Satcher, Jr., and L.W. Hrubesh, in *Handbook of Porous Solids*, edited by F. Schuth, K.S.W. Sing, and J. Weitkamp (Wiley-VCH, Weinheim, 2002), and references therein.

<sup>3</sup>Z. Zhu, L.Y. Tsung, and M. Tomkiewicz, *J. Chem. Phys.* **99**, 15945 (1995).

<sup>4</sup>O. Masson, V. Rieux, T. Guinebretiere, and A. Dauger, *Nanostruct. Mater.* **7**, 725 (1996).

<sup>5</sup>V. Luca, S. Djajanti, and R.F. Howe, *J. Phys. Chem. B* **102**, 10650 (1998).

<sup>6</sup>T.L. Hanley, V. Luca, I. Pickering, and R.F. Howe, *J. Phys. Chem. B* **106**, 1153 (2002).

<sup>7</sup>H. Yoshitake, T. Sugihara, and T. Tatsumi, *Phys. Chem. Chem. Phys.* **5**, 767 (2003).

<sup>8</sup>L. Soriano, M. Abbate, J. Vogel, J.C. Fuggle, A. Fernandez, A.R. Gonzalez-Eliphe, M. Sacchi, and J.M. Sanz, *Surf. Sci.* **290**, 427 (1993).

<sup>9</sup>V.S. Lusvardi, M.A. Barteau, J.G. Chen, J. Eng, Jr., B. Fruhberger, and A. Teplyakov, *Surf. Sci.* **397**, 237 (1998).

<sup>10</sup>J. Biener, M. Baumer, J. Wang, and R.J. Madix, *Surf. Sci.* **450**, 12 (2000).

<sup>11</sup>I. Khubeis, R. Fromknecht, and O. Meyer, *Phys. Rev. B* **55**, 136 (1997).

<sup>12</sup>T. Hartmann, L.M. Wang, W.J. Weber, N. Yu, K.E. Sickafus, J.N. Mitchell, C.J. Wetteland, M.A. Nastasi, M.G. Hollander, N.P. Baker, C.R. Evans, J.R. Tesmer, and C.J. Maggiore, *Nucl. Instrum. Methods Phys. Res. B* **141**, 398 (1998).

<sup>13</sup>F.X. Li, M. Ishimaru, P. Lu, I.V. Afanasyev-Charkin, and K.E. Sickafus, *Nucl. Instrum. Methods Phys. Res. B* **166-167**, 314 (2000).

<sup>14</sup>To our knowledge, the values of the surface binding energies (*E<sub>b</sub>*), which largely determine the ion-beam-induced sputtering yield, are unknown for TiO<sub>2</sub>. However, TRIM code simulations (version SRIM-2003.17) (Ref. 15) show that, even if *E<sub>b</sub>* were as low as 2 eV for both O and Ti, the total sputtering yield would

be ~11 atoms/ion. In this case, only an ~17-Å-thick layer would be sputtered for a dose of 1.5 × 10<sup>15</sup> cm<sup>-2</sup>. Ion irradiation under such conditions is expected to have a minor effect on the stoichiometry of the ~100–200-Å-thick near-surface layer probed in total electron yield XANES measurements around O *K* and Ti *L*<sub>2,3</sub> edges.

<sup>15</sup>J.F. Ziegler, J.P. Biersack, and U. Littmark, *The Stopping and Range of Ions in Solids* (Pergamon, New York, 1985).

<sup>16</sup>We use the term “unrelaxed” as it is widely accepted to describe semiconductors amorphized by ion bombardment and not subjected to any high-temperature processing (Ref. 17).

<sup>17</sup>See, for example, S. Roorda, W.C. Sinke, J.M. Poate, D.C. Jacobson, S. Dierker, B.S. Dennis, D.J. Eaglesham, F. Spaepen, and P. Fuoss, *Phys. Rev. B* **44**, 3702 (1991), and references therein.

<sup>18</sup>J.J. Jia, T.A. Callcott, J. Yurkas, A.W. Ellis, F.J. Himpsel, M.G. Samant, J. Stohr, D.L. Ederer, J.A. Carlisle, E.A. Hudson, L.J. Terminello, D.K. Shuh, and R.C.C. Perera, *Rev. Sci. Instrum.* **66**, 1394 (1995).

<sup>19</sup>R. Brydson, H. Sauer, W. Engel, J.M. Thomas, E. Zeitler, N. Kosugi, and H. Kuroda, *J. Phys.: Condens. Matter* **1**, 797 (1989); R. Brydson, B.G. Williams, W. Engel, H. Sauer, E. Zeitler, and J.M. Thomas, *Solid-State Electron.* **64**, 609 (1987).

<sup>20</sup>Fitting spectra with Gaussian functions gave poor results, supporting that peak widths in this study are largely determined by the lifetime broadening rather than by experimental resolution.

<sup>21</sup>D.W. Fischer, *Phys. Rev. B* **5**, 4219 (1972).

<sup>22</sup>F.M.F. de Groot, J. Faber, J.J.M. Michiels, M.T. Czyzyk, M. Abbate, and J.C. Fuggle, *Phys. Rev. B* **48**, 2074 (1993).

<sup>23</sup>R. Ruus, A. Kikas, A. Saar, A. Ausmees, E. Nommiste, J. Aarik, A. Aidla, T. Uustare, and I. Martinson, *Solid State Commun.* **104**, 199 (1997).

<sup>24</sup>G. van der Laan, *Phys. Rev. B* **41**, 12366 (1990).

<sup>25</sup>J.A. Tossell, D.J. Vaughan, and K.H. Johnson, *Am. Mineral.* **59**, 319 (1974).

<sup>26</sup>F.M.F. de Groot, J.C. Fuggle, B.T. Thole, and G.A. Sawatzky, *Phys. Rev. B* **41**, 928 (1990).

<sup>27</sup>F.M.F. de Groot, M.O. Figueiredo, M.J. Basto, M. Abbate, H. Petersen, and J.C. Fuggle, *Phys. Chem. Miner.* **19**, 140 (1992).

- <sup>28</sup>L.D. Finkelstein, E.I. Zabolotzky, M.A. Korotin, S.N. Shamin, S.M. Butorin, E.Z. Kurmaev, and J. Nordgren, *X-Ray Spectrom.* **31**, 414 (2002).
- <sup>29</sup>It should be noted that the relative intensities of peaks in Fig. 4 could be largely affected by the background subtraction procedure, given the uncertainty in the shape of the peaks and the background.
- <sup>30</sup>J.P. Crocombette and F. Jollet, *J. Phys.: Condens. Matter* **6**, 10811 (1994).
- <sup>31</sup>See, for example, a review by W. Ulrici, in *Modern Problems in Condensed Matter Sciences*, edited by Yu.E. Perlin and M. Wagner (North-Holland, Amsterdam, 1984), Vol. 7, p. 439.
- <sup>32</sup>S. Munnix and M. Schmeits, *Phys. Rev. B* **30**, 2202 (1984).
- <sup>33</sup>L.A. Grunes, R.D. Leapman, C.N. Wilker, R. Hoffmann, and A.B. Kunz, *Phys. Rev. B* **25**, 7157 (1982); L.A. Grunes, *ibid.* **27**, 2111 (1983).
- <sup>34</sup>K.M. Glassford and J.R. Chelikowsky, *Phys. Rev. B* **46**, 1284 (1992).
- <sup>35</sup>S.-D. Mo and W.Y. Ching, *Phys. Rev. B* **51**, 13 023 (1995).
- <sup>36</sup>A. Munoz-Paez and P. Malet, *Appl. Surf. Sci.* **56-58**, 873 (1992).
- <sup>37</sup>G. Antonioli, D. Bersani, P.P. Lottici, I. Mazini, G. Gnappi, and A. Montenero, *Nucl. Instrum. Methods Phys. Res. B* **97**, 198 (1995).